ACS APPLIED MATERIALS & INTERFACES

Research Article

www.acsami.org

Localized Ion-Beam Irradiation-Induced Wrinkle Patterns

Hae-Chang Jeong,[†] Hong-Gyu Park,[†] Ju Hwan Lee, and Dae-Shik Seo*

Information Display Device Laboratory, Department of Electrical and Electronic Engineering, Yonsei University, 50 yonsei-ro, Seodaemun-gu, Seoul 120-749, Republic of Korea

Supporting Information

ABSTRACT: We observe a localized irradiation-induced wrinkle pattern on poly(dimethylsiloxane) (PDMS) via a long pattern mask. Localized ion-beam irradiation induces an inhomogeneous wrinkle pattern on the treated region. To confirm the inhomogeneity of the entire wrinkle pattern, its morphology was investigated using optical microscopy, which revealed separated regions in the wrinkle pattern. We used atomic force microscopy for quantitative analysis of the wrinkle pattern morphology and analyzed the angular distribution and the direction of compressive stress of the irradiated area. We confirmed the direction of stress release along the distance from the edges, and we achieved control of the orientation of the wrinkle pattern by altering the width of the irradiated area. Investigation of the inhomogeneities in a localized wrinkle formation provides an understanding of the formation mechanism to enhance its performance and application in various fields.

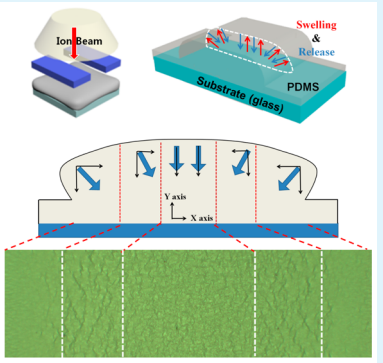

KEYWORDS: *local treatment, inhomogeneous pattern, ion beam, wrinkle, poly(dimethylsiloxane)*

INTRODUCTION

A wrinkle structure can be obtained by inducing a deformation between the top and underlying layers.[1] This response results from the minimization of both the bending energy of the stiff top layer and the stretching energy of the soft underlying foundation.[2,3] Because of the disruption of the symmetric formation between the adjacent layers in a material, the occurrence of wrinkling is typically considered undesirable. However, the wrinkling phenomenon in nano/macrodevice fabrication has been studied in-depth from an engineering perspective because it is a useful tool to enhance the optical,[4,5] electrical,[6] and mechanical[7,8] performances of numerous devices. Moreover, as with wrinkles encountered in daily life, the control of spontaneous wrinkle structures is an attractive and promising technique for surface patterning[1] and can be applied to various areas of interest, including stretchable electronics,[9] microlens array fabrication,[10] liquid-crystal alignment[4,11] and microfluidics,[12] and colloidal particle aggregation.[13] Therefore, numerous theoretical studies have been devoted to understanding the formation mechanism of wrinkle patterns to potentially control the inaccuracy in wrinkle formation and, consequently, the performance of wrinkle patterns in applications.

There are several methods of wrinkle formation, such as metal deposition,[1] plasma treatment,[14] multistep plasma thermal treatment,[15] and ion-beam (IB) irradiation[11,16,17] of soft materials (especially, IB irradiation is a powerful method to fabricate surface nanopatterning of various materials).[18−20] To expand their availability and usage, other approaches, such as the application of a prestrain,[8] curving of the substrate,[21] and localized formation,[11,22] have been developed. However, these approaches induce the occurrence of inhomogeneities on wrinkle patterns. Our group has previously examined the effect of locally irradiating a wrinkle pattern and detected the inhomogeneous wrinkle pattern along the distance from the center region on an irradiated surface.[11] These inhomogeneities are attributed to the difference in the locally induced strains on the surface. Therefore, we are expected to control its inhomogeneities by figuring out the locally induced strain on the surface. For potential applications in a wrinkle pattern, the control of inhomogeneities on wrinkle patterns is important to stabilize the performances on wrinkle applications as with the control of wrinkle characterization such as the wrinkle wavelength and amplitude.

In this paper, we present the experimental observation of localized irradiation-induced inhomogeneities in a wrinkle on the length of the pattern mask with poly(dimethylsiloxane) (PDMS). To confirm the inhomogeneities on the entire wrinkle pattern, its morphology was investigated by optical microscopy (OM). From the morphology information obtained by OM, we observed various regions on the surface. Atomic force microscopy (AFM) was used to determine the mechanism of wrinkle formation of the separated regions by analyzing the angular distribution and direction of compressive stress on the visually separated areas. Additionally, by altering the width of the irradiated area, we could control the internal compressive stress applied to the wrinkle, thus inducing a high orientational order in the wrinkle. Investigation of the inhomogeneities in localized wrinkle formation provides an

Received: August 3, 2015
Accepted: October 2, 2015
Published: October 2, 2015

DOI: 10.1021/acsami.5b07147
ACS Appl. Mater. Interfaces 2015, 7, 23216−23222

understanding of the formation mechanism to enhance its performance and application in various fields.

RESULTS AND DISCUSSION

Figure 1a shows the OM image of the entire surface exposed to the IB via the mask pattern. The resultant wrinkle patterns do

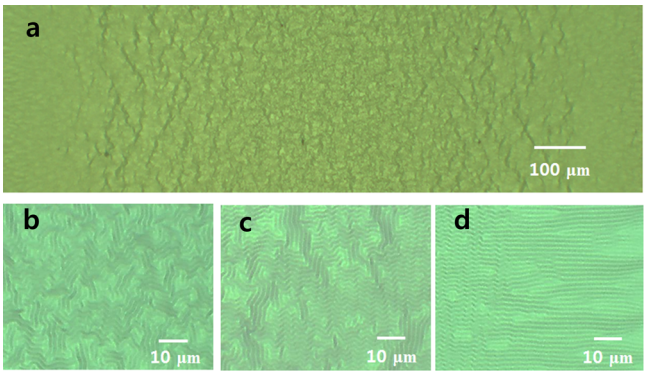

Figure 1. OM images of the localized IB irradiation-induced wrinkle pattern using a patterning mask of 1 mm width: (a) entire wrinkle pattern surface; (b) central area; (c) area approximately 300 μm from the edge; (d) area near the edge.

not exhibit an entirely homogeneous morphology, thus intrinsically introducing divisions on the surface. The IB irradiation modified the chemical composition of the skin layer and created a stiff skin layer.[17] The newly formed skin layer bound to the soft substrates induced the difference in the mechanical properties between adjacent layers, leading to compressive stress and in-plane compressive strain on the surface. Beyond a critical point, the compressive stress caused by the stiff skin layer leads to an out-of-plane deformation, thereby forming a wrinkle structure on soft materials. When the wrinkle was formed, the direction of the compressive stress determined the wrinkle morphology.[2] Equally contributing stress along the axes caused the randomly oriented pattern. When the symmetry of the stress along the axes was disrupted, the wrinkle morphology was altered into a parallel pattern by the relative difference in the stress along the axes. Random labyrinth wrinkles were observed in the central region exposed through the mask pattern (Figure 1b). When approaching the edges, the adjacent wrinkles merged in a direction perpendicular to the bifurcation section (Figure 1c). Subsequently, organization into a one-dimensional (1D) structure and herringbone stripes occurred at the edge of the side (Figure 1d). The 1D structure and several bifurcation points appeared at the edge of the exposed region/at the bifurcation points, the wrinkles merged or separated into several branches, and a herringbone pattern appeared. The localized IB irradiation via the mask pattern may have induced the directional difference in the compressive stress along the region, leading to inhomogeneous patterns on the surface.

To discriminate among the morphologies and the position, we investigated the wrinkle morphology using AFM, as shown in Figure 2a. Region A shows a random labyrinth structure that is the center of the mask pattern exposed to the IB. According to a previous study, the orientation of the wrinkle stripes is determined by the ratio of the compressive strain along the axes and should minimize the free energy. Although the equally contributing strain induced an isotropic wrinkle pattern, a small difference in the induced strain causes the preferred stripes to

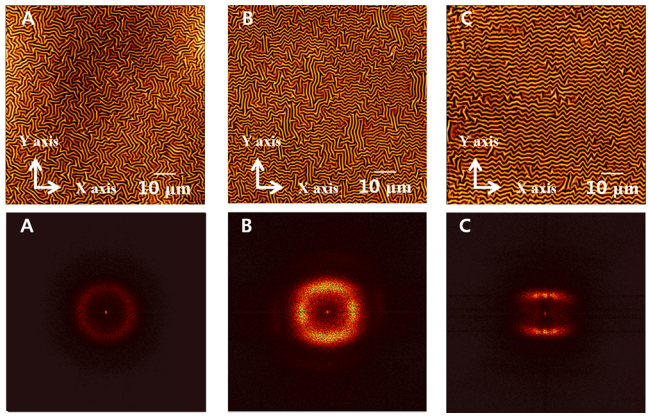

Figure 2. Investigation of the wrinkle morphology of separated areas via AFM. (a, top) AFM images at the center A, the central area B approximately 300 μm from the edge, and edge area C approximately 100 μm from the edge. (b, bottom) 2D FFT analysis at areas A–C.

form in the θ direction relative to the direction of the smaller applied strain. The 0.8 compressive strain ratio satisfies the minimum free energy at the symmetrical angles of +45° and −45°, indicating that the perpendicular stripes are related to the differences in the induced compressive strain along the x and y axes. Area B shows two dominant directional wrinkle patterns: one pattern is parallel to the widthwise direction of the mask pattern, and the second pattern is perpendicular to the first direction. The +45° direction relative to the widthwise direction is termed "α", and the −45° direction is termed "β". A small difference in the compressive stress along the α and β directions may induce perpendicular stripes, and as the distance from the center increases, the compressive stress changes from isotropic to anisotropic. The herringbone structure, which is the minimum energy configuration in stripe characterization,[23] stretched toward the edge. The difference in the morphological characteristics is remarkably confirmed by two-dimensional (2D) fast Fourier transform (FFT) analysis, as shown in Figure 2b. Area A shows equally distributed 2D FFT graphs, indicating random labyrinth patterns. At area B, four separate sections can be observed, indicating a perpendicularly alternating pattern. Finally, the opposing sides of 2D FFT indicate an anisotropic pattern. These results are consistent with the morphological characteristics.

Figure 3 shows the angular distribution and formation mechanism of each wrinkle pattern in the different areas. From the AFM images shown in Figure 2, line-segment detection was performed using *MATLAB*. The segment of the wrinkle pattern that is defined by the bifurcation points separated along different directions and various angle points was detected (see the Supporting Information, Figure S1). We extracted the length of the line and the inclination angle relative to the widthwise direction of the mask pattern to confirm the degree of wrinkle alignment. The line segments were fitted with a maximum deviation of two pixels from the original edge. To confirm the degree of wrinkle alignment, we derived the order parameter equation of the wrinkle segment, which is given by eq 1, as follows:

$$S = \frac{\langle 3\cos^2\theta - 1\rangle}{2} \quad (1)$$

θ is the inclination angle of the segments, here relative to the widthwise direction of the mask pattern, i.e., the x axis in Figure

DOI: 10.1021/acsami.5b07147
ACS Appl. Mater. Interfaces 2015, 7, 23216–23222

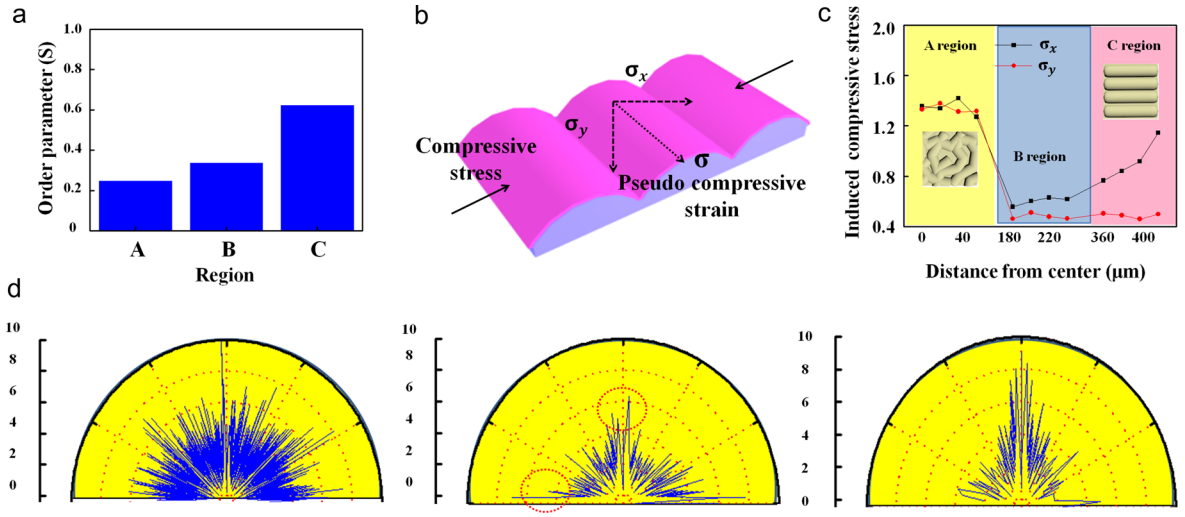

Figure 3. Numerical analysis of the wrinkle pattern. (a) Order parameter of the wrinkle pattern along the areas. A is the area at the center of the irradiated region. B is a central area 300 μm away from the edge. C is an edge area approximately 100 μm from the edge boundary. (b) Schematic of the pseudocompressive strain. (c) Induced pseudocompressive strain as a function of the area. (d) Polar coordinates of the wrinkle and the length of the wrinkle segment and inclination angles relative to the widthwise mask pattern.

2a. The values numerically show the average angular distribution of all of the wrinkle segments. Because this distribution is low, the value of the order parameter (S) approaches 1, indicating that the wrinkles were perfectly aligned. Otherwise, the evenly distributed angles of the wrinkled segment, such as the random labyrinth pattern, have lower values of S. Aligned liquid crystals have a typical S value ranging from 0.3 to 0.8. The S value of the central area A is 0.247, indicating randomly oriented patterns, and this value is consistent with the random labyrinth wrinkle structure shown in Figure 2. Perpendicularly alternating patterns are observed in area B, whose S value is 0.34. One of the alternating patterns at B is parallel to the widthwise direction, thus increasing the S value; however, the other alternating pattern is perpendicular, and this decreases the S value to 0.34, which is approximately equal to that of an incidence angle of 41°. The S value of area C is 0.62 and is within the range of that of aligned liquid crystals. The preferred stripes are 30° off the widthwise direction on average. This indicates the 1D herringbone structure in which the average incidence angle is 30°, and this result is consistent with the wrinkle pattern morphologies shown in Figure 2. Therefore, upon approaching the edge, the S value increases and the wrinkle segment is ordered in the widthwise direction. IB irradiation creates a stiff skin layer that induces a compressive stress along the opposing side, thereby inducing an out-of-plane deformation and forming a wrinkle valley (i.e., a wrinkle segment) perpendicular to the direction of the compressive stress (Figure 3b). However, when an external strain is applied to the surface,[2] the wrinkle valley is formed parallel to the strain, which is itself perpendicular to the compressive stress direction, and its pattern morphology is controlled by the relative difference in strain along the axes. Therefore, although there is no application of external forces and the compressive stress is only due to the stiff skin layer, it can be assumed that a pseudocompressive strain is applied on the surface parallel to the wrinkle valley; i.e., a compressive stress exists along the perpendicular direction and forms a wrinkle valley. This mechanism can allow the approximate degree of compressive stress to be measured using the length of the wrinkle valley and its incidence angle.

$$\sigma_x = h \cos \theta$$

$$\sigma_y = h \sin \theta$$

h is the length of the wrinkle valley, and x and y represent the width and length of the mask pattern, respectively. We assume that σ is the pseudocompressive strain induced by the compressive stress that forms a wrinkle valley. Using the line-segment-detection feature in *MATLAB* and quiver arrangement, the pseudocompressive strain was obtained. We separated the four sections of each region along the x direction from the left side of the AFM images in Figure 2. σ_x and σ_y are nearly equal at A (Figure 3c). An average of 1.3 μm of pseudocompressive strain was induced, indicating that a random labyrinth pattern was induced from an equal stress at area A. At area B, the compressive stress is not equally distributed along the x and y directions, and the ratio of σ_y to σ_x is approximately 0.8. Because the aforementioned strain difference determines the wrinkle pattern, the 0.8 strain ratio allowed the two inclination angles to satisfy the minimum free energy at ±45°.[24] The result of the pseudocompressive assumption is consistent with the aforementioned strain difference studies. This indicates that the perpendicularly alternating pattern is caused by disruption of the symmetric stress and that the direction of the pseudocompressive strain may be 45° relative to the orientation of the pattern. When the distance from the center is increased, the direction of the compressive stress applied to the surface is gradually altered. Near the edge, the pseudocompressive strain is more dominant along the x direction than along the y direction. A large σ_x, compared to σ_y, is induced in area C, and a 1D herringbone pattern is induced along the x direction. A recent energy calculation study explained that a herringbone pattern has a lower elastic energy than a stripe pattern under biaxial compression because the herringbone pattern relieves film compression in both directions, although the directional differences in the stress are large. Although biaxial stress exists through the surface, when approaching the edge, the difference between the pseudocompressive strain along the axes is gradually larger, and thus the morphology of the wrinkle

DOI: 10.1021/acsami.5b07147
ACS Appl. Mater. Interfaces 2015, 7, 23216−23222

pattern is affected by the distance from the center, inducing an anisotropic pattern. These results enable identification of the direction of the compressive stress on inhomogeneous wrinkle patterns.

The angular distribution of each section allows visualization of the degree of wrinkle alignment (Figure 3d). Area A shows an equal distribution at all angles. Area B does not show equally distributed angles for the wrinkle patterns; however, long lines are observed at approximately 0° and 90° relative to the widthwise direction of the mask pattern, i.e., the x and y axes, respectively. In area C, the dominant angles are within ±30° relative to the preferred direction. The angular distribution also supports the result of a pseudocompressive strain.

A schematic of the wrinkle morphology using the mask pattern is shown in Figure 4. Three different regions can be

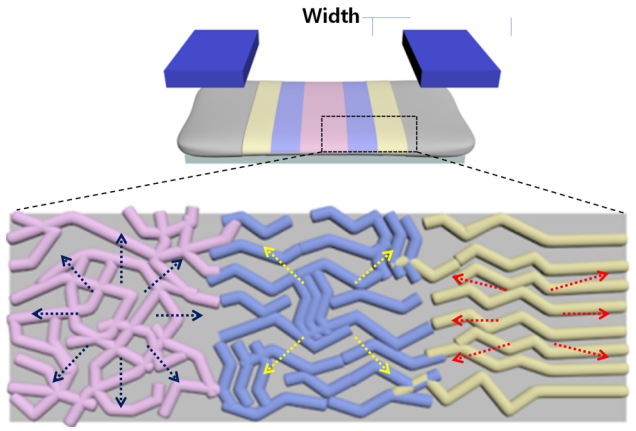

Figure 4. Schematic of the localized IB irradiation-induced wrinkle pattern. The dotted arrows indicate the direction of the pseudocompressive strain.

observed on the surface. As the distance from the center to the edge of the wrinkle structure increases, the random labyrinth structure morphs into a 1D structure. The different morphologies on the same level plane were caused by a gradual variation of the internal stress along a specific direction.[14] According to the aforementioned pseudocompressive strain and angular distribution, the compressive stress in a localized IB irradiation-induced wrinkle is affected by the distance from the edge. An equibiaxial stress, illustrated by blue dotted arrows, is generated at the center area, indicating a pseudocompressive strain. The equally distributed pseudocompressive strain varies with increasing distance from the center. The symmetry of the compressive stress is broken and a perpendicularly alternating wrinkle pattern is formed between the center and edge. Perpendicularly alternating wrinkles are attributed to the generation of differences in the compressive stress from isotropic stress.[24] The yellow dotted arrows illustrate the direction of the pseudocompressive strain on the perpendicularly alternating stripes. Concerning the energy aspect of parallel wrinkle formation, a herringbone structure is in a lower energy state than a 1D structure because of the relaxation in all directions in contrast with the 1D relaxation in one direction. When proceeding to the edge boundary, the herringbone structure morphs into a 1D structure. Therefore, the stress at the center is released in all directions, thereby inducing a random labyrinth structure; subsequently, as the distance from the center increases, the relaxation direction converges by applying an anisotropic strain along the direction of the 1D pattern. Near the edges, the stress is predominantly released in one direction.

To confirm the relationship between the distance from the edge and the inhomogeneous wrinkle pattern, the IB-irradiated surface was altered using mask patterns of different width sizes and investigated by OM (Figure 5). The width of the mask was

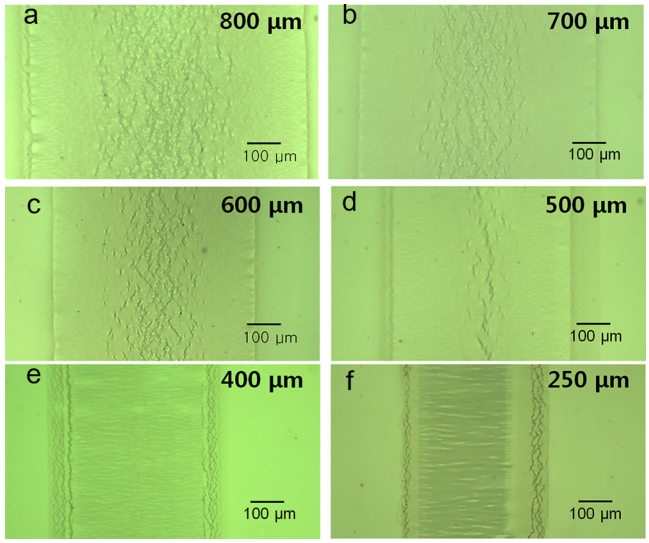

Figure 5. Investigation of the localized IB irradiation-induced wrinkle pattern with various widths of the mask pattern. The widths of the mask patterns are (a) 800, (b) 700, (c) 600, (d) 500, (e) 400, and (f) 250 μm.

decreased from 800 to 300 μm. At 1 mm, two different wrinkle patterns emerged on the surface, which are represented in Figure 5 by the shaded central regions and bright edge regions. However, around the center, the wrinkle pattern can be separated into two different sections, one with an inclination angle of 90° and a second with a random labyrinth structure. At the edge, the bright regions represent the parallel and herringbone structures. When the exposure width was decreased to 800 μm, the labyrinth structure disappeared first. Subsequently, up to an exposure width of 400 μm, a perpendicularly alternating pattern was predominantly observed and the area of the shaded region gradually decreased. The shaded region gradually disappeared, and at an exposure width of 500 μm, a narrow shaded region was observed along the lengthwise direction. At 400 μm, the shaded area eventually disappeared and a 1D structure was observed.

Figure 6 shows statistical data on the area and pattern morphology. In Figure 6, the numerical data on the y axis represents the distance from the edge up to half the width size, and the x axis represents the variation in the width of the mask pattern. Up to a width of the mask pattern of 400 μm, only parallel stripes were observed. Between a width of 400 and 200 μm, the parallel pattern was observed around the edge, and a perpendicular pattern appeared around the center, which is depicted by the shaded region in Figure 5. Up to 800 μm, the perpendicular pattern was observed after the position where the parallel pattern was observed. This perpendicularly alternating pattern was also observed approximately 200 μm from the parallel pattern, and this area was constant throughout the variation of the width of the mask pattern. As the width increased, the parallel and perpendicular patterns morphed into the labyrinth pattern at the center. The labyrinth pattern

DOI: 10.1021/acsami.5b07147
ACS Appl. Mater. Interfaces 2015, 7, 23216−23222

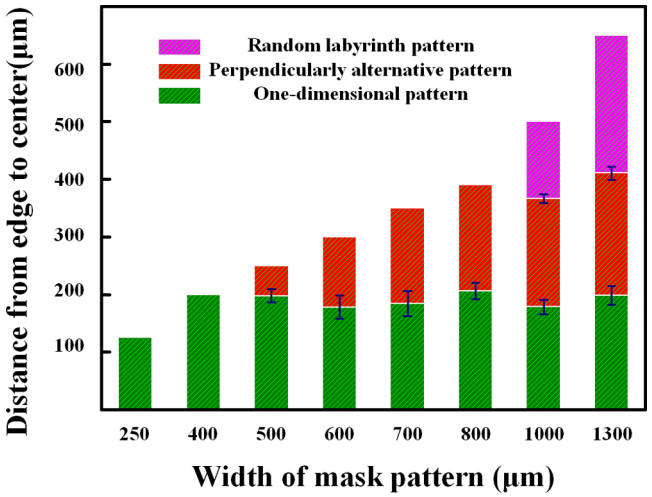

Figure 6. Coverage of different wrinkle patterns as a function of the width of the mask pattern. The coverage of different wrinkle patterns is shown along the *y* axis from the edge to the center.

emerged at a distance of approximately 400 μm from the edge. Eventually, the edge boundary affected the inhomogeneity of the surface by inducing a difference in the compressive stress along the widthwise and lengthwise directions of the patterning mask. The area separated by changes in the orientation of the wrinkle patterns is constant, irrespective of the width size of the pattern mask.

To examine the coverage of different wrinkle patterns in detail, we additionally changed the IB intensity and investigated the wrinkle pattern coverage and wrinkle wavelength with various IB intensities. The coverage pattern data of various IB intensities were obtained by using different widths of the mask (see the Supporting Information, Figure S2). To form a wrinkle structure, the IB power intensity needed to be larger than a critical wrinkle-formation threshold. Under 800 eV, the IB intensity was not sufficient to form a wrinkle structure.[11,25] Starting at 800 eV, a wrinkle was formed and similar pattern steps from the edge were observed irrespective of the IB intensity (Figure 7a). Parallel, perpendicular, and random patterns were observed as the distance from the edge increased. However, the various IB intensities exhibited different coverages of the wrinkle pattern. At an IB intensity of 800 eV, the coverage of the parallel pattern, which is observed at the near edge, averaged 66 μm, and there was a steady increase in the coverage of the 1D pattern as the IB intensity increases. The coverage of the parallel pattern for intensities of 1100, 1400, 1700, and 2000 eV averaged 81.5, 115.2, 156.4, and 190.4 μm, respectively. As with the parallel pattern, the perpendicular pattern exhibited an increase in the coverage in which the coverage of 800, 1100, 1400, 1700, and 2000 eV averaged 65.7, 70.6, 103.1, 132.8, and 191.6 μm., respectively. Figure 7b exhibits the wrinkle wavelength as a function of the IB intensity. A strong IB intensity increases in the wrinkle wavelength, which is similar to that with the coverage of the wrinkle pattern at various IB intensities (Table 1; see the Supporting Information, Figure S3). IB irradiation changed the surface of PDMS into an oxidation state by penetrating the ion particle. The penetration depth depends on the IB intensities,[26] which is the main factor in controlling the wrinkle wavelength.[16,17,22,25] We found that the tendencies of the wrinkle wavelength and coverage of the parallel pattern are similar as a function of the IB intensity in Figure 7. Table 1 exhibits the ratio between the coverage of the

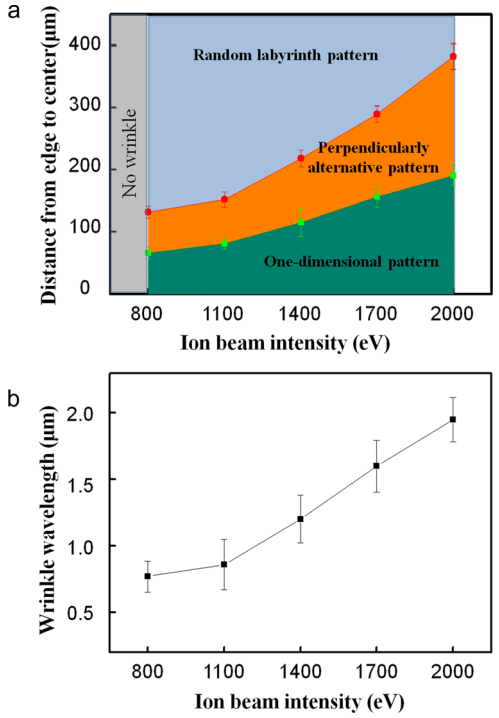

Figure 7. (a) Coverage of different wrinkle patterns as a function of the IB intensity along the *y* axis from the edge to the center. (b) Variation in the wrinkle wavelength as a function of the IB intensity.

Table 1. Wrinkle Wavelength (λ), Coverage of the Parallel Pattern (C_p), and Ratio of λ to d_p at Various IB Intensities

	IB intensity (eV)				
	800	1100	1400	1700	2000
λ (μm)	0.75	0.86	1.2	1.62	1.95
C_p (μm)	66	81.5	115.2	156.4	190.4
C_p/λ	88.1	94.7	96	96.5	97.7

parallel pattern and the wrinkle wavelength (C_p/λ). C_p/λ ranged from 88 to 98. Considering deviation of the wrinkle wavelength and coverage, the deviation of C_p/λ with various IB intensities is $\pm$20 and C_p/λ of 88−98 seems to be within the experimental range.

Figure 8 proposes a localized IB irradiation-induced wrinkle formation mechanism that involves different wrinkle patterns at separated regions. Bowden et al. described that thin-metal-deposited PDMS on the substrate create a wrinkle structure because of the swelling mechanism induced by heat.[1] In a similar case, our previous work confirmed that IB-irradiated PDMS on substrates forms a wrinkle structure by the swelling mechanism;[11] when an accelerated ion reached the surface of PDMS, a skin layer was modified and the energy of IB caused an expansion of PDMS; subsequently, the formed skin layer induced a contraction of the swelled PDMS, thereby forming a wrinkle structure. Figure 8a illustrates that swelling on locally irradiated PDMS was limited by the boundary region; the red line represents the direction of expansion, and blue line represents the direction of contraction. Because of the limited expansion induced by the boundary, the direction of expansion near the boundary spreads out in the *x* axis, which is the widthwise direction of the mask (Figure 8a). During the contraction process, in the direction opposite to that of expansion, contraction occurs and the compressive strain is

DOI: 10.1021/acsami.5b07147
ACS Appl. Mater. Interfaces 2015, 7, 23216−23222

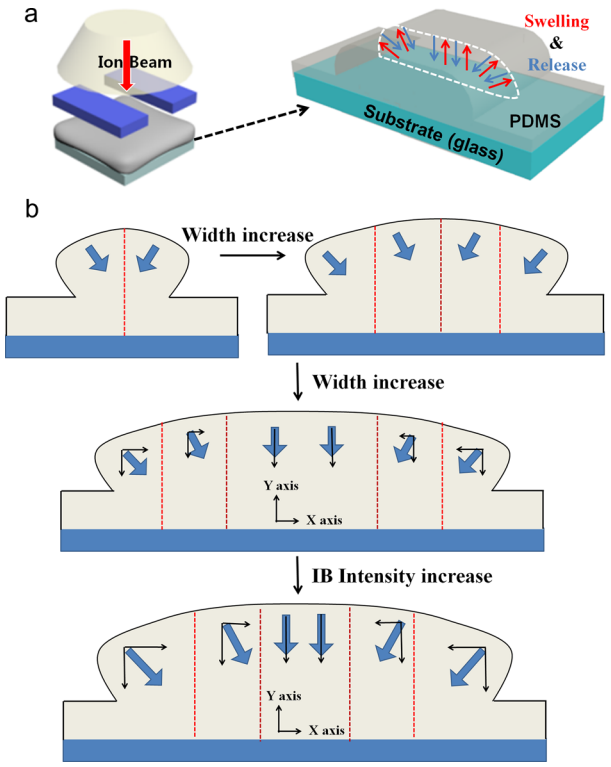

Figure 8. Schematic diagram of the mechanism of inhomogeneous wrinkle formation. (a) Localized IB irradiation on PDMS using the mask pattern, with swelling occurring at the exposed region. (b) Cross section with an increase in the exposure width, subsequently increasing the IB intensity.

generated. This dominant compressive strain induced by limited expansion allows for a parallel wrinkle pattern along the x axis (Figure 8b). As the irradiated region is widened, x axis−compressive strain gradually decrease far from the boundary. After the irradiated region is sufficiently increased, x axis−compressive strain disappear on the center region and only biaxial stress relief exists on the surface, forming a random wrinkle pattern. We experimentally confirmed that the effect of x axis−compressive strain is constant irrespective of the exposure width size with constant IB intensity.

In the case of variation in the IB intensity, we confirmed that the coverage of the parallel pattern gradually increases as the IB intensity increases. A strong IB intensity forces the accelerated ion with high energy to reach the surface. The accelerated ion with high energy transfers its energy to PDMS. PDMS with high energy expands more by the swelling mechanism, and the effect of x axis−compressive strain also increases with the ratio between the coverage of the parallel pattern and the wrinkle wavelength, the value of which is on average 95 and almost constant irrespective of the IB intensity (Figure 8b).

CONCLUSION

In summary, we confirm the localized IB irradiation-induced inhomogeneity of wrinkle patterns by observing a pseudocompressive strain. Additionally, the inhomogeneity of the wrinkle pattern is affected by the distance from the edge. As the distance from the center increases, the relaxation direction converges by applying an anisotropic strain along the direction of the 1D pattern. At the center, the stress is released in all directions, thereby inducing a random labyrinth structure; around the edge of the boundary, the stress is primarily released in one direction. The localized irradiation leads to a relatively different compressive stress on the surface, inducing a different orientation of the wrinkle pattern. By analyzing the characteristics of a localized irradiation-induced wrinkle, we achieved control of the orientational wrinkle pattern by altering the width of the irradiated area. This study on the inhomogeneity of a wrinkle pattern using a localized treatment can be potentially applied to nano/macrofabrication, the arrangement of nanomaterials, and flexible electron devices. By observing and controlling the morphology of spontaneously generated wrinkle patterns, we expect to broaden the view of the formation of inhomogeneous wrinkle patterns.

METHOD

PDMS Preparation. PDMS samples were prepared using a mixture of elastomers and cross-linkers in a mass ratio of 10:1 (Sylgard-184, Dow Corning). The mixture was placed in a plastic box and stirred to remove trapped air bubbles. Prepared PDMS was spin-coated onto 20 × 30 mm indium−tin oxide glass substrates at 3000 rpm for 30 s and then cured at 65 °C for 4 h, resulting in a cross-linked PDMS network.

Localized Irradiation via a Mask Pattern. A Duo PI Gatron ion-beam system was employed for the Ar^+ IB irradiation. The PDMS samples were placed in a high-vacuum chamber under a working pressure of ~3×10^{-4} Pa and an argon gas flow rate of less than 1 sccm. The PDMS surface was exposed to the IB in a digital mode with acceleration voltages of 2 keV and an ion current of 1 mA. The localized irradiation was achieved via a long rectangular patterning mask. The widths of the mask were 250 μm, 400 μm, 500 μm, 600 μm, 700 μm, 800 μm, 1 mm, and 1.3 mm. The length of the mask was 2 cm.

Investigation of the Localized Wrinkle Pattern Using AFM and OM. The surface morphology of the localized irradiation-induced wrinkle pattern was observed using AFM (JPK Instruments AG, NanoWizard1). Subsequently, 2D FFT analysis was performed on the AFM images to confirm the characteristics of the wrinkle pattern. The coverage investigation of different wrinkle formation was conducted using OM (Ted Pella, Inc., Motic BA310MET).

Calculation of the Characteristics of the Wrinkle Pattern. We used line-segment detection in *MATLAB* to analyze the AFM images. The line segments were fitted with a maximum deviation of two pixels from the original edge. Each wrinkle segment was represented by a detected line segment; these segments represented the inclination angles relative to the widthwise patterning mask and the length of the wrinkle segment. We calculated the order parameter, polar angles, and pseudocompressive strain using the numerical data obtained by line-segment detection and quiver arrangement.

ASSOCIATED CONTENT

Supporting Information

The Supporting Information is available free of charge on the ACS Publications website at DOI: 10.1021/acsami.5b07147.

Experimental details, AFM and OM images, and surface morphology (PDF)

AUTHOR INFORMATION

Corresponding Author

*E-mail: dsseo@yonsei.ac.kr.

Author Contributions

†These authors contributed equally.

Notes

The authors declare no competing financial interest.

DOI: 10.1021/acsami.5b07147
ACS Appl. Mater. Interfaces 2015, 7, 23216−23222

REFERENCES

(1) Whitesides, G. M.; Bowden, N.; Brittain, S.; Evans, A. G.; Hutchinson, J. W. Spontaneous Formation of Ordered Structures in Thin Films of Metals Supported on an Elastomeric Polymer. *Nature* **1998**, *393*, 146−149.

(2) Cerda, E.; Mahadevan, L. Geometry and Physics of Wrinkling. *Phys. Rev. Lett.* **2003**, *90*, 074302.

(3) Genzer, J.; Groenewold, J. Soft Matter with Hard Skin: From Skin Wrinkles to Templating and Material Characterization. *Soft Matter* **2006**, *2*, 310−323.

(4) Ohzono, T.; Monobe, H.; Yamaguchi, R. Y.; Shimizu, Y.; Yokoyama, H. Dynamics of Surface Memory Effect in Liquid Crystal Alignment on Reconfigurable Microwrinkles. *Appl. Phys. Lett.* **2009**, *95*, 014101.

(5) Cendula, P.; Kiravittaya, S.; Schmidt, O. Electronic and Optical Properties of Quantum Wells Embedded in Wrinkled Nanomembranes. *J. Appl. Phys.* **2012**, *111*, 043105.

(6) Wang, B.; Zhang, Y.; Zhang, H.; Chen, Z.; Xie, X.; Sui, Y.; Li, X.; Yu, G.; Hu, L.; Jin, Z.; Liu, X. Wrinkle-dependent Hydrogen Etching of Chemical Vapor Deposition-grown Graphene Domains. *Carbon* **2014**, *70*, 75−80.

(7) Yang, P.; Baker, R. M.; Henderson, J. H.; Mather, P. T. In Vitro Wrinkle Formation via Shape Memory Dynamically Aligns Adherent Cells. *Soft Matter* **2013**, *9*, 4705−4714.

(8) Li, B.; Cao, Y.-P.; Feng, X.-Q.; Gao, H. Mechanics of Morphological Instabilities and Surface Wrinkling in Soft Materials: A Review. *Soft Matter* **2012**, *8*, 5728−5745.

(9) Khang, D.-Y.; Jiang, H.; Huang, Y.; Rogers, J. A. A Stretchable Form of Single-crystal Silicon For High-performance Electronics on Rubber Substrates. *Science* **2006**, *311*, 208−212.

(10) Chan, E. P.; Crosby, A. J. Fabricating Microlens Arrays by Surface Wrinkling. *Adv. Mater.* **2006**, *18*, 3238−3242.

(11) Jeong, H.-C.; Park, H.-G.; Lee, J. H.; Jung, Y. H.; Jang, S. B.; Seo, D.-S. Homogeneous Self-aligned Liquid Crystals on Wrinkled-wall Poly(dimethylsiloxane) via Localised Ion-beam Irradiation. *Sci. Rep.* **2015**, *5*, 8641.

(12) Ohzono, T.; Monobe, H. Morphological Transformation of a Liquid Micropattern on Dynamically Tunable Microwrinkles. *Langmuir* **2010**, *26*, 6127−6132.

(13) Pazos-Peréz, N.; Ni, W.; Schweikart, A.; Alvarez-Puebla, R. A.; Fery, A.; Liz-Marzán, L. M. Highly Uniform SERS Substrates Formed by Wrinkle-confined Drying of Gold Colloids. *Chem. Sci.* **2010**, *1*, 174−178.

(14) Breid, D.; Crosby, A. J. Effect of Stress State on Wrinkle Morphology. *Soft Matter* **2011**, *7*, 4490−4496.

(15) Lee, W.-K.; Engel, C. J.; Huntington, M. D.; Hu, J.; Odom, T. W. Controlled Three-Dimensional Hierarchical Structuring by Memory-Based, Sequential Wrinkling. *Nano Lett.* **2015**, *15*, 5624−5629.

(16) Evensen, H. T.; Jiang, H.; Gotrik, K. W.; Denes, F.; Carpick, R. W. Transformations in Wrinkle Patterns: Cooperation between Nanoscale Cross-Linked Surface Layers and the Submicrometer Bulk in Wafer-Spun, Plasma-Treated Polydimethylsiloxane. *Nano Lett.* **2009**, *9*, 2884−2890.

(17) Park, H.-G.; Jeong, H.-C.; Jung, Y. H.; Seo, D.-S. Control of The Wrinkle Structure on Surface-Reformed Poly(dimethylsiloxane) via Ionbeam Bombardment. *Sci. Rep.* **2015**, *5*, 12356.

(18) Castro, M.; Cuerno, R. Hydrodynamic Approach to Surface Pattern Formation by Ion Beams. *Appl. Surf. Sci.* **2012**, *258*, 4171−4178.

(19) Moreno-Barrado, A.; Castro, M.; Gago, R.; Vazquez, L.; Munoz-Garcıa, J.; Redondo-Cubero, A.; Galiana, B.; Ballesteros, C.; Cuerno, R. Nonuniversality due to Inhomogeneous Stress in Semiconductor Surface Nanopatterning by Low-energy Ion-beam Irradiation. *Phys. Rev. B: Condens. Matter Mater. Phys.* **2015**, *91*, 155303.

(20) Kumar, T.; Kumar, A.; Lalla, N. P.; Hooda, S.; Ojha, S.; Verma, S.; Kanjilal, D. Role of Ion Beam Induced Solid Flow in Surface Patterning of Si (1 0 0) using Ar ion beam irradiation. *Appl. Surf. Sci.* **2013**, *283*, 417−421.

(21) Stoop, N.; Lagrange, R.; Terwagne, D.; Reis, P. M.; Dunkel, J. Curvature-induced Symmetry Breaking Determines Elastic Surface Patterns. *Nat. Mater.* **2015**, *14*, 337−342.

(22) Moon, M.-W.; Her, E.-K.; Oh, K. H.; Lee, K.-R.; Vaziri, A. Sculpting on Polymers using Focused Ion Beam. *Surf. Coat. Technol.* **2008**, *202*, 5319−5324.

(23) Chen, X.; Hutchinson, J. W. Herringbone Buckling Patterns of Compressed Thin Films on Compliant Substrates. *J. Appl. Mech.* **2004**, *71*, 597−603.

(24) Gao, Y. F.; Lu, W.; Suo, Z. A Mesophase Transition in a Binary Monolayer on a Solid Surface. *Acta Mater.* **2002**, *50*, 2297−2308.

(25) Moon, M.-W.; Lee, S.-H.; Sun, J.-Y.; Oh, K. H.; Vaziri, A.; Hutchinson, J. W. Wrinkled Hard Skins on Polymers Created by Focused Ion Beam. *Proc. Natl. Acad. Sci. U. S. A.* **2007**, *104*, 1130.

(26) Torrisi, L.; Gammino, S.; Mezzasalma, A. M.; Badziak, J.; Parys, P.; Wolowski, J.; Woryna, E.; Krása, J.; Láska, L.; Pfeifer, M.; Rohlena, K.; Boody, F. P. Implantation of Ions Produced by The Use of High Power Iodine Laser. *Appl. Surf. Sci.* **2003**, *217*, 319−331.

DOI: 10.1021/acsami.5b07147
ACS Appl. Mater. Interfaces 2015, 7, 23216−23222